Acta Mech 228, 1303–1319 (2017)
DOI 10.1007/s00707-016-1781-4

ORIGINAL PAPER

Y. Kiani

# Buckling of FG-CNT-reinforced composite plates subjected to parabolic loading

Received: 6 August 2016 / Published online: 5 December 2016


**Abstract** It is known that the distribution of stresses in a rectangular plate is the same as the applied stresses on the boundaries when the loading is uniform or linearly varying. For other types of compressive loads, for instance parabolic compressive loading, the distribution of stresses in the plate is different from the applied loads at the boundaries of the plate. For such conditions, to obtain the buckling loads of the plate, an accurate prebuckling analysis should be performed. The present research aims to obtain the buckling loads and buckling pattern of composite plates reinforced with carbon nanotubes with uniform or functionally graded distribution across the plate thickness. The properties of the composite media are obtained based on a modified rule of mixtures approach with the introduction of efficiency parameters. First-order shear deformation plate theory is used to approximate the plate kinematics. The plate is subjected to uniaxial compressive loads which vary as parabolic functions across the width of the plate. At first, using the Ritz method and Airy stress function formulation, the distribution of stress resultants in the plate domain is obtained as a two-dimensional elasticity formulation. Afterwards, by means of the Chebyshev polynomials as the basic functions of the Ritz solution method, an eigenvalue problem is established to obtain the buckling load and buckling shape of the plate. Comparison studies are provided to assure the accuracy of the presented formulation for isotropic homogeneous and cross-ply laminated plates. Afterwards, parametric studies are performed for composite plates reinforced with carbon nanotubes.

## 1 Introduction

Rectangular plates are a part of more complex structures, and due to the loading condition of the structure, the applied load on the rectangular plate may not be uniform. Nonuniform distribution of in-plane loads is observed in the case of an I beam or wide-flanged beam subjected to a bending moment at the ends or lateral loads on the flange, aircraft wings, stiffened plates in the ship structures, and multi-storey buildings by the adjoining structures. For nonuniform distribution of compressive in-plane loads acting on the plate edges, understanding the buckling behaviour becomes important and should be studied to grasp the general information on the response of the structure which leads to a reliable design.

A literature survey reveals that the linear buckling problem of rectangular plates subjected to uniform compression is well documented in the open literature. In this type of loading, the differential equations associated with the onset of buckling are linear with constant coefficients. Furthermore, the distribution of in-plane stresses within the plate is similar to the applied edge loads. In comparison with uniform edge loading, less researches are available on the buckling behaviour of rectangular plates subjected to nonuniform edge loadings. The reason is that the governing equations for such problems have nonconstant coefficients. Among the buckling problems with nonuniform edge loading, linearly varying loads are more observed since in this

Y. Kiani (✉)
Faculty of Engineering, Shahrekord University, Shahrekord, Iran
E-mail: y.kiani@eng.sku.ac.ir; y.kiani@aut.ac.ir

case the prebuckling loads are the same as the applied in-plane loads. For other types of nonuniform loading, the distribution of in-plane stresses in the plate is different from the applied in-plane loads, and to obtain the critical buckling loads of the plate, prebuckling loads should be obtained accurately. This is the reason of the limited number of investigations dealing with the buckling of rectangular plates with nonuniform compression.

Based on a mesh-free formulation, Chen and Liew [1] obtained the critical buckling loads of homogeneous and functionally graded material plates subjected to point force, partial compression, and parabolic loading. This research is based on the first-order plate theory and a mesh-free method based on the radial basis functions. Based on a two-dimensional generalised differential quadrature, Wang et al. [2] obtained the buckling loads of thin rectangular plates based on the classical plate theory. In this research, the plate is subjected to uniaxial parabolic in-plane loads. Prior to the eigenvalue analysis to obtain the buckling loads of the plate, a two-dimensional elasticity problem is solved to extract the distribution of in-plane stresses induced by the nonuniform compression. Tang and Wang [3] reported the buckling loads of symmetrically laminated rectangular plates subjected to parabolic loading. A Ritz formulation with the aid of Airy stress function formulation is developed to obtain the distribution of normal and shear stresses within the plate. Afterwards, the buckling problem of the plate is formulated using the two-dimensional generalised differential quadrature method suitable for arbitrary combinations of clamped and simply supported boundary conditions. Panda and Ramachandra [4] developed, respectively, a Ritz and a Galerkin procedure to obtain the prebuckling and buckling stresses of the isotropic homogeneous and cross-ply laminated plates. In the prebuckling state, a three-parameter stress function comprising polynomial functions satisfying all of the force boundary conditions on the edges of the plate is constructed. The unknown parameters are obtained via the minimum potential energy criterion. The obtained prebuckling forces are inserted into the stability equations of a thick plate whose solution is estimated by means of the beam function. The developed solution, also, may be used for arbitrary combinations of clamped and simply supported boundary conditions. Ramachandra and Panda [5] developed their previous investigation [4] to analyse the dynamic stability of rectangular plates loaded by a parabolically varying load. Similar to the previous investigation of the authors [4], Ritz and Galerkin methods are used, to obtain the distribution of in-plane forces and instability regions, respectively. Ovesy and Fazilati [6] developed a finite strip method to distinguish the instability regions of a cylindrical shell panel subjected to compressive loads which vary as a parabolic function of the panel width. Dey et al. [7] obtained the linear buckling loads and also the postbuckling equilibrium path of rectangular sandwich plates subjected to either partial or parabolic loading. In this research, each of the layers has its own kinematics, and the continuity of the displacements between the layers is satisfied. In this analysis, Dey et al. [7] extended the previous formulation of [4,5] suitable for not only the parabolic but also the partial loading. Panda and Ramachandra [8] obtained the prebuckling, buckling and postbuckling responses of rectangular cross-ply laminated plates subjected to uniaxial compression. Panda and Ramachandra [9] presented a solution based on the Galerkin method suitable for a postbuckling analysis of cylindrical panels with all edges simply supported and subjected to uniaxial or biaxial parabolic loading. To trace the equilibrium path, the Newton–Raphson method in conjunction with the Riks procedure is implemented.

Carbon nanotubes (CNTs) have exceptional thermomechanical properties which makes them a candidate for the reinforcement of composites [10]. It is reported that nonuniform distribution of CNTs may be achieved by a powder metallurgy process [11]. Therefore, the concept of FGMs and CNTs may be achieved together via a nonuniform distribution of CNTs through a specific direction [12]. This class of materials is known as functionally graded carbon nanotube-reinforced composites (FG-CNTRC).

With the introduction of FG-CNTRC materials, many researches are devoted to the stability analysis of FG-CNTRC structures. Among the reported works on stability of FG-CNTRC plates, one may refer to the stability analysis of skew plates made of FG-CNTRC based on a first-order plate theory and an element-free formulation carried out by Zhang et al. [13] an investigation of Lei et al. [14] for a stability analysis of FG-CNTRC rectangular plates based on the element-free kp-Ritz method, a buckling analysis of Malekzadeh and Shojaee [15] for laminated plates in a arbitrary quadrilateral shape made from FG-CNTRC layers using a generalised differential quadrature, the development of an element-free method for a buckling analysis of skew-shaped FG-CNTRC plates resting on a two-parameter elastic foundation performed by Lei et al. [16], and the buckling and postbuckling of FG-CNTRC plates [17] and sandwich plates with FG-CNTRC face sheets [18] with simply supported edges based on a two-step perturbation technique. However, in all of these mentioned works, the in-plane applied loads are of uniform type.

The aim beyond the present research is to extend the available works on the stability analysis of FG-CNTRC plates. Buckling load factors are obtained for a rectangular shape composite plate reinforced with single-walled carbon nanotubes. At first, a prebuckling analysis is performed to obtain the accurate distribution

of in-plane loads due to the applied parabolic compression. Afterwards, stability equations are discretized with the aid of the Ritz method where the shape functions are constructed in terms of the Chebyshev polynomials. The resulting eigenvalue problem is established and solved for various combinations of boundary conditions, aspect ratio, side-to-thickness ratio, CNT volume fraction, and CNT dispersion profile. It is shown that the buckling loads of the plate are affected by the CNT characteristics significantly.

## 2 Basic formulation

An FG-CNTRC rectangular plate is considered is this research. Thickness, width and length of the plate are denoted by, $h$, $b$, and $a$, respectively. The conventional Cartesian coordinate system with its origin located at the centre of the plate where $-0.5a \leq x \leq +0.5a$, $-0.5b \leq y \leq +0.5b$, and $-0.5h \leq z \leq +0.5h$ is considered. The geometric characteristics of the plate, applied coordinate system, and applied compressive loads are depicted in Fig. 1.

The plate is made from a polymeric matrix reinforced with single-walled carbon nanotubes (SWCNT). The distribution of SWCNT across the plate thickness may be uniform (referred to as UD) or functionally graded (referred to as FG). In this research, two types of mid-plane symmetric FG distribution of CNTs and the UD case are considered. FG-O and FG-X CNTRC are the functionally graded distribution of carbon nanotubes across the thickness direction of the rectangular composite plate.

Generally, the effective mechanical properties of the FG-CNTRC rectangular plate are obtained using the well-known homogenisation schemes, such as Mori-Tanaka scheme [19] or the rule of mixtures [20]. For the sake of simplicity, in the present research, the rule of mixtures is used to obtain the properties of the composite plate. However, to account for the scale-dependent properties of nanocomposite media, efficiency parameters are introduced. The refined rule of mixture approach which contains the efficiency parameters has been used extensively in analysis of FG-CNTRC beams [21–24], plates [25–27], panels [28–30], and shells [31–33]. According to the rule, the effective material properties may be written as [12,34]

$$\begin{aligned} E_{11} &= \eta_1 V_{CN} E_{11}^{CN} + V_m E^m, \\ \frac{\eta_2}{E_{22}} &= \frac{V_{CN}}{E_{22}^{CN}} + \frac{V_m}{E^m}, \\ \frac{\eta_3}{G_{12}} &= \frac{V_{CN}}{G_{12}^{CN}} + \frac{V_m}{G^m}. \end{aligned} \tag{1}$$

In the above equations, $\eta_1$, $\eta_2$, and $\eta_3$ are the so-called efficiency parameters which as mentioned earlier are introduced to account for the size-dependent material properties of the plate. These constants are chosen to equal the obtained values of Young's modulus and shear modulus from the present modified rule of mixtures with the results obtained according to the molecular dynamics simulations [34]. Besides, $E_{11}^{CN}$, $E_{22}^{CN}$, and $G_{12}^{CN}$ are the elasticity modulus and shear modulus of SWCNTs, respectively. Furthermore, $E^m$ and $G^m$ indicate the corresponding properties of the isotropic matrix.

In Eq. (1), the volume fraction of CNTs and matrix is denoted by $V_{CN}$ and $V_m$, respectively, which satisfy the condition

$$V_{CN} + V_m = 1. \tag{2}$$

As mentioned earlier, two types of functionally graded CNTRC plates are considered. These types along with the UD type are the considered patterns of CNT dispersion through the thickness of the plate. In Table 1, the distribution function of CNTs across the plate thickness is provided.

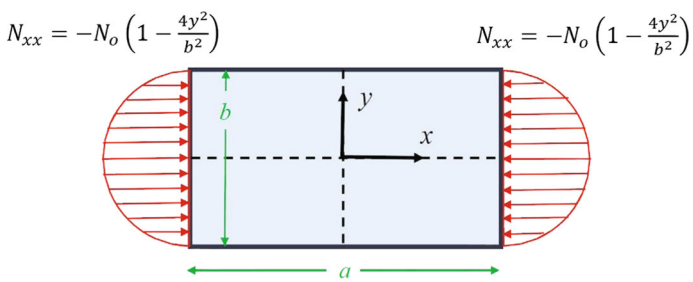


**Fig. 1** Coordinate system, dimensions, and the schematic of the applied compressive loads

**Table 1** Volume fraction of CNTs as a function of the thickness coordinate for various cases of CNTs distribution.

| CNTs distribution | $V_{CN}$ |
|---|---|
| UD CNTRC | $V_{CN}^{*}$ |
| FG-O CNTRC | $2V_{CN}^{*}\left(1-2\frac{\lvert z\rvert}{h}\right)$ |
| FG-X CNTRC | $4V_{CN}^{*}\frac{\lvert z\rvert}{h}$ |

It is easy to check from Table 1 that all of these types have the same value of volume fraction. The total volume fraction across the plate thickness in all of these cases is equal to $V_{CN}^{*}$. In FG-X type, the distribution of CNTs is maximum near the top and bottom surfaces, whereas the mid-plane is free of CNTs. For FG-O, however, top and bottom surfaces are free of CNTs, and the mid-surface of the plate is enriched with CNTs. In UD type, each surface of the plate though the thickness has the same volume fraction of CNTs.

The effective Poisson's ratio depends weakly on position [31,34] and is expressed as

$$\nu_{12} = V_{CN}^{*}\nu_{12}^{CN} + V_m\nu^m. \tag{3}$$

First-order shear deformation theory (FSDT) of plates suitable for moderately thick and even thick plates is used in this study to estimate the kinematics of the plate [35]. According to the FSDT, the displacement components of the plate may be written in terms of the characteristics of the mid-surface of the plate and cross-sectional rotations as

$$\begin{aligned} u\left(x,y,z\right) &= u_0\left(x,y\right) + z\varphi_x\left(x,y\right), \\ v\left(x,y,z\right) &= v_0\left(x,y\right) + z\varphi_y\left(x,y\right), \\ w\left(x,y,z\right) &= w_0\left(x,y\right). \end{aligned} \tag{4}$$

In the above equation, $u$, $v$, and $w$ are the through-the-length, through-the-width and through-the-thickness displacements, respectively. Mid-plane characteristics of the plate are designated with a subscript 0. Besides, transverse normal rotations about the $x$ and $y$ axes are denoted by $\varphi_y$ and $\varphi_x$, respectively.

Following the FSDT, in-plane strain components are written in terms of mid-plane strains and change in curvatures. Besides, through-the-thickness shear strain components are assumed to be constant. Therefore, one may write

$$\begin{Bmatrix} \varepsilon_{xx} \\ \varepsilon_{yy} \\ \gamma_{xy} \\ \gamma_{xz} \\ \gamma_{yz} \end{Bmatrix} = \begin{Bmatrix} \varepsilon_{xx0} \\ \varepsilon_{yy0} \\ \gamma_{xy0} \\ \gamma_{xz0} \\ \gamma_{yz0} \end{Bmatrix} + z \begin{Bmatrix} \kappa_{xx} \\ \kappa_{yy} \\ \kappa_{xy} \\ \kappa_{xz} \\ \kappa_{yz} \end{Bmatrix}. \tag{5}$$

In this study, a rectangular plate under the action of nonuniform compression is under investigation. It is known that a stability analysis should be performed under geometrically nonlinear conditions. However, when only the buckling state is under consideration and the prebuckling state of the structure is deflectionless, a linear analysis suffices. In such conditions, the problem may be formulated under geometrically linear conditions, and the effect of the prebuckling loads may be invoked into the total potential energy of the system as a work done by the external loads.

Considering the above discussions, the linear strain–displacement relations may be written as

$$\begin{Bmatrix} \varepsilon_{xx0} \\ \varepsilon_{yy0} \\ \gamma_{xy0} \\ \gamma_{xz0} \\ \gamma_{yz0} \end{Bmatrix} = \begin{Bmatrix} u_{0,x} \\ v_{0,y} \\ u_{0,y} + v_{0,x} \\ \varphi_x + w_{0,x} \\ \varphi_y + w_{0,y} \end{Bmatrix}, \tag{6}$$

and the components of change in curvature compatible with the FSDT are

$$\begin{Bmatrix} \kappa_{xx} \\ \kappa_{yy} \\ \kappa_{xy} \\ \kappa_{xz} \\ \kappa_{yz} \end{Bmatrix} = \begin{Bmatrix} \varphi_{x,x} \\ \varphi_{y,y} \\ \varphi_{x,y} + \varphi_{y,x} \\ 0 \\ 0 \end{Bmatrix} \tag{7}$$

where in the above equations $()_{,x}$ and $()_{,y}$ denote the derivatives with respect to the $x$ and $y$ directions, respectively.

For linear elastic materials, the stress field may be expressed as a linear function of the strain field as

$$\begin{Bmatrix} \sigma_{xx} \\ \sigma_{yy} \\ \tau_{yz} \\ \tau_{xz} \\ \tau_{xy} \end{Bmatrix} = \begin{bmatrix} Q_{11} & Q_{12} & 0 & 0 & 0 \\ Q_{12} & Q_{22} & 0 & 0 & 0 \\ 0 & 0 & Q_{44} & 0 & 0 \\ 0 & 0 & 0 & Q_{55} & 0 \\ 0 & 0 & 0 & 0 & Q_{66} \end{bmatrix} \begin{Bmatrix} \varepsilon_{xx} \\ \varepsilon_{yy} \\ \gamma_{yz} \\ \gamma_{xz} \\ \gamma_{xy} \end{Bmatrix}. \tag{8}$$

In this equation, $Q_{ij}$'s $(i, j = 1, 2, 4, 5, 6)$ are the reduced material stiffness coefficients compatible with the plane stress conditions and are obtained as follows [25]:

$$\begin{aligned} &Q_{11} = \frac{E_{11}}{1 - \nu_{12}\nu_{21}}, \quad Q_{22} = \frac{E_{22}}{1 - \nu_{12}\nu_{21}}, \quad Q_{12} = \frac{\nu_{21}E_{11}}{1 - \nu_{12}\nu_{21}}, \\ &Q_{44} = G_{23}, \quad Q_{55} = G_{13}, \quad Q_{66} = G_{12}. \end{aligned} \tag{9}$$

Stress resultants of the FSDT may be obtained upon integration of the stress field through the thickness. Stress resultant components in this case become [35]

$$\begin{Bmatrix} N_{xx} \\ N_{yy} \\ N_{xy} \\ M_{xx} \\ M_{yy} \\ M_{xy} \\ Q_{xz} \\ Q_{yz} \end{Bmatrix} = \int_{-0.5h}^{+0.5h} \begin{Bmatrix} \sigma_{xx} \\ \sigma_{yy} \\ \tau_{xy} \\ z\sigma_{xx} \\ z\sigma_{yy} \\ z\tau_{xy} \\ \kappa\tau_{xz} \\ \kappa\tau_{yz} \end{Bmatrix} \mathrm{d}z. \tag{10}$$

In the above equation, $\kappa$ is the shear correction factor of the FSDT. For FG-CNTRC beams, plates and shells, the value of $\kappa$ is used as $\kappa = \dfrac{5}{6 - \nu_{12}}$.

Substitution of Eq. (8) into Eq. (10) with the simultaneous aid of Eqs. (4)–(7) and (9) generates the stress resultants in terms of the mid-surface characteristics of the plate as

$$\begin{Bmatrix} N_{xx} \\ N_{yy} \\ N_{xy} \\ M_{xx} \\ M_{yy} \\ M_{xy} \\ Q_{yz} \\ Q_{xz} \end{Bmatrix} = \begin{bmatrix} A_{11} & A_{12} & 0 & B_{11} & B_{12} & 0 & 0 & 0 \\ A_{12} & A_{22} & 0 & B_{12} & B_{22} & 0 & 0 & 0 \\ 0 & 0 & A_{66} & 0 & 0 & B_{66} & 0 & 0 \\ B_{11} & B_{12} & 0 & D_{11} & D_{12} & 0 & 0 & 0 \\ B_{12} & B_{22} & 0 & D_{12} & D_{22} & 0 & 0 & 0 \\ 0 & 0 & B_{66} & 0 & 0 & D_{66} & 0 & 0 \\ 0 & 0 & 0 & 0 & 0 & 0 & \kappa A_{44} & 0 \\ 0 & 0 & 0 & 0 & 0 & 0 & 0 & \kappa A_{55} \end{bmatrix} \begin{Bmatrix} \varepsilon_{xx0} \\ \varepsilon_{yy0} \\ \gamma_{xy0} \\ \kappa_{xx} \\ \kappa_{yy} \\ \kappa_{xy} \\ \gamma_{yz0} \\ \gamma_{xz0} \end{Bmatrix}. \tag{11}$$

In the above equation, the stiffness components $A_{ij}$, $B_{ij}$, and $D_{ij}$ indicate the stretching, bending–stretching, and bending stiffnesses, respectively, which are calculated by

$$(A_{ij}, B_{ij}, D_{ij}) = \int_{-0.5h}^{+0.5h} (Q_{ij}, zQ_{ij}, z^2Q_{ij})\mathrm{d}z. \tag{12}$$

## 3 Prebuckling analysis

As mentioned earlier, for the case of parabolic compression, the distribution of in-plane loads is different from the applied loads at the edges. Therefore, to obtain the accurate buckling loads of the rectangular plate subjected to parabolic load compression, a prebuckling analysis should be studied first. In the prebuckling analysis, rotations and deflections are equal to zero. Consequently, only the in-plane displacement components are present, and transverse shear strains are equal to zero before buckling. Displacement components may be obtained by applying the virtual displacement principle. In the prebuckling state, one may write

$$\delta U^0 = \int_{-0.5a}^{+0.5a} \int_{-0.5b}^{+0.5b} \int_{-0.5h}^{+0.5h} \left( \sigma_{xx}^0 \delta \varepsilon_{xx0}^0 + \sigma_{yy}^0 \delta \varepsilon_{yy0}^0 + \tau_{xy}^0 \delta \gamma_{xy0}^0 \right) \mathrm{d}z\mathrm{d}y\mathrm{d}x = 0 \tag{13}$$

where upon integration on thickness it is reduced to

$$\delta U^0 = \int_{-0.5a}^{+0.5a} \int_{-0.5b}^{+0.5b} \left( N_{xx}^0 \delta \varepsilon_{xx0}^0 + N_{yy}^0 \delta \varepsilon_{yy0}^0 + N^0 \delta \gamma_{xy0}^0 \right) \mathrm{d}y\mathrm{d}x = 0 \tag{14}$$

where a superscript zero indicates the prebuckling state of the plate. In the above equation, the influence of the applied compressive load is included into the first term in the integrand. Recalling the applied loads on the boundary, the boundary conditions of the plate are

$$\begin{aligned} &x = \pm a/2 : N_{xx}^0 = -N_0 \left( 1 - \frac{4y^2}{b^2} \right), \quad N_{xy}^0 = 0, \\ &y = \pm b/2 : N_{xy}^0 = 0, \quad N_{yy}^0 = 0. \end{aligned} \tag{15}$$

Recalling Eq. (11), the components of strain in the prebuckling state may be obtained in terms of stresses in the prebuckling state as

$$\begin{aligned} \varepsilon_{xx0}^0 &= a_{11} N_{xx}^0 + a_{12} N_{yy}^0, \\ \varepsilon_{yy0}^0 &= a_{12} N_{xx}^0 + a_{22} N_{yy}^0, \\ \gamma_{xy0}^0 &= a_{66} N_{xy}^0 \end{aligned} \tag{16}$$

where the following definitions apply:

$$\begin{aligned} a_{11} &= \frac{A_{22}}{A_{11}A_{22} - A_{12}^2}, \\ a_{22} &= \frac{A_{11}}{A_{11}A_{22} - A_{12}^2}, \\ a_{12} &= \frac{-A_{12}}{A_{11}A_{22} - A_{12}^2}, \\ a_{66} &= \frac{1}{A_{66}}. \end{aligned} \tag{17}$$

The virtual energy of the plate mentioned previously in Eq. (16) may be written in terms of the Airy stress function. The components of stress resultants in terms of the Airy stress function are

$$N_{xx}^0 = F_{,yy}, \qquad N_{yy}^0 = F_{,xx}, \qquad N_{xy}^0 = -F_{,xy}. \tag{18}$$

Finally, substitution of Eqs. (16) and (18) into Eq. (14) results in the expression of virtual strain energy in terms of the stress function as

$$\delta U^0 = \int_{-0.5a}^{+0.5a} \int_{-0.5b}^{+0.5b} \left( a_{11} F_{,yy} \delta F_{,yy} + a_{22} F_{,xx} \delta F_{,xx} + a_{12} F_{,xx} \delta F_{,yy} + a_{12} F_{,yy} \delta F_{,xx} + a_{66} F_{,xy} \delta F_{,xy} \right) \mathrm{d}y\mathrm{d}x = 0 \tag{19}$$

where the boundary conditions (15) in terms of the Airy stress function may be written as

$$x = \pm a/2 : F_{,yy} = -N_0\left(1 - \frac{4y^2}{b^2}\right), \quad F_{,xy} = 0,$$
$$y = \pm b/2 : F_{,xy} = 0, \quad F_{,xx} = 0. \tag{20}$$

Here the Ritz method is used to solve Eq. (19) with regard to boundary conditions (20). The approximate stress function is considered in the following form:

$$F = -\frac{1}{2}N_0 y^2\left(1 - \frac{2y^2}{3b^2}\right) + \left(1 - \frac{4x^2}{a^2}\right)^2\left(1 - \frac{4y^2}{b^2}\right)^2\left(C_0 + C_1x^2 + C_2y^2 + C_3x^4 + C_5y^4 + C_6x^2y^2\right). \tag{21}$$

It is easy to check that the above stress function exactly satisfies all of the required boundary conditions of Eq. (20). The above estimation of the stress function contains six unknown coefficients which should be determined upon substitution of Eq. (21) into (19) and minimising the expression with respect to these unknowns. It should be noted that only even powers in the second part of the stress function are considered since the applied edge load is symmetric with respect to the coordinate system. Obtaining the constant coefficients $C_i$, $i = 1, 2, \ldots, 6$, the stress function is constructed with the aid of Eq. (21). Afterwards, the distribution of in-plane stresses is obtained by means of the definition of the Airy stress function in Eq. (18).

## 4 Buckling analysis

The stability equations of the plate may be obtained with the aid of the static version of the Hamilton principle [35]. For the buckling analysis, one may write

$$\delta(U + V) = 0 \tag{22}$$

where $\delta U$ is the virtual strain energy of the plate which may be calculated as

$$\delta U = \int_{-0.5a}^{+0.5a}\int_{-0.5b}^{+0.5b}\int_{-0.5h}^{+0.5h}\left(\sigma_{xx}\delta\varepsilon_{xx} + \sigma_{yy}\delta\varepsilon_{yy} + \tau_{xy}\delta\gamma_{xy} + \kappa\tau_{xz}\delta\gamma_{xz} + \kappa\tau_{yz}\delta\gamma_{yz}\right)\mathrm{d}z\mathrm{d}y\mathrm{d}x, \tag{23}$$

and $\delta V$ is the potential energy due to the prebuckling loads which may be written as

$$\delta V = -\int_{-0.5a}^{+0.5a}\int_{-0.5b}^{+0.5b}\left(N^0_{xx}w_{0,x}\delta w_{0,x} + N^0_{yy}w_{0,y}\delta w_{0,y} + N^0_{xy}w_{0,y}\delta w_{0,x} + N^0_{xy}w_{0,x}\delta w_{0,y}\right)\mathrm{d}y\mathrm{d}x. \tag{24}$$

While the complete set of stability equations and the associated boundary conditions may be obtained by the application of the Green–Gauss theorem to the expression (22), energy-based methods also may be used to solve the stability equations associated with the functional (22). In the present research, the conventional Ritz method with Chebyshev basis polynomials is used to extract the equilibrium equations in a matrix representation. Accordingly, each of the essential variables may be expanded via Chebyshev polynomials and auxiliary functions such that

$$u_0(x, y) = R^u(x, y)\sum_{i=1}^{N_x}\sum_{j=1}^{N_y}U_{ij}P_i(x)P_j(y),$$
$$v_0(x, y) = R^v(x, y)\sum_{i=1}^{N_x}\sum_{j=1}^{N_y}V_{ij}P_i(x)P_j(y),$$
$$w_0(x, y) = R^w(x, y)\sum_{i=1}^{N_x}\sum_{j=1}^{N_y}W_{ij}P_i(x)P_j(y),$$
$$\varphi_x(x, y) = R^x(x, y)\sum_{i=1}^{N_x}\sum_{j=1}^{N_y}X_{ij}P_i(x)P_j(y),$$

$$\varphi_y(x, y) = R^y(x, y) \sum_{i=1}^{N_x} \sum_{j=1}^{N_y} Y_{ij} P_i(x) P_j(y) \tag{25}$$

where in the above equation $P_i(x)$ and $P_j(y)$ are the $i$-th and $j-$th Chebyshev polynomials of the first kind which are defined by

$$\begin{aligned} P_i(x) &= \cos((i-1)\arccos(2x/a)), \\ P_j(y) &= \cos((j-1)\arccos(2y/b)). \end{aligned} \tag{26}$$

Besides, functions $R^\alpha(x, y), \alpha = u, v, w, x, y$ are the boundary functions corresponding to the essential boundary conditions. It is known that in Ritz family methods, the adoption of a shape function depends only on the essential boundary conditions. Three types of boundary conditions are used in this study, i.e. clamped (C), simply supported (S), and free (F). For a clamped edge, all of the out-of-plane essential variables are restrained, while for a simply supported edge lateral displacement and tangential slope are restrained. For a free edge, none of the out-of-plane essential variables are restrained at a edge. Therefore, the essential variables at a edge may be written as

$$\begin{aligned} &\text{For a clamped edge:} \\ &x = \pm a/2 : w_0 = \varphi_x = \varphi_y = 0, \\ &y = \pm b/2 : w_0 = \varphi_x = \varphi_y = 0; \\ &\text{For a simply supported edge:} \\ &x = \pm a/2 : w_0 = \varphi_y = 0, \\ &y = \pm b/2 : w_0 = \varphi_x = 0; \\ &\text{For a free edge:} \\ &x = \pm a/2 : -, \\ &y = \pm b/2 : -. \end{aligned} \tag{27}$$

The shape functions of the Ritz method should be chosen according to the above essential variables. All of the Chebyshev functions are nonzero at both ends of the interval. Therefore, auxiliary functions $R^\alpha, \alpha = u, v, w, x, y$ should satisfy the essential boundary conditions on each edge of the plate. Each of the functions $R^\alpha, \alpha = u, v, w, x, y$ may be written as

$$R^\alpha(x, y) = \left(1 + \frac{2x}{a}\right)^p \left(1 - \frac{2x}{a}\right)^q \left(1 + \frac{2y}{b}\right)^r \left(1 - \frac{2y}{b}\right)^s. \tag{28}$$

Each of the variables $p, q, r$, and $s$ depends on the essential boundary conditions and is equal to zero or one. For instance, in a plate with clamped boundaries on $x = -0.5a$ and $x = +0.5a$, simply supported at $y = -0.5b$ and free at $y = +0.5b$, auxiliary functions are

$$\begin{aligned} R^u(x, y) &= 1, \\ R^v(x, y) &= 1, \\ R^w(x, y) &= \left(1 + \frac{2x}{a}\right)\left(1 - \frac{2x}{a}\right)\left(1 + \frac{2y}{b}\right), \\ R^x(x, y) &= \left(1 + \frac{2x}{a}\right)\left(1 - \frac{2x}{a}\right)\left(1 + \frac{2y}{b}\right), \\ R^y(x, y) &= \left(1 + \frac{2x}{a}\right)\left(1 - \frac{2x}{a}\right). \end{aligned} \tag{29}$$

Finally, substitution of Eq. (25) into Eqs. (23) and (24) and inserting the results into the statement of the Hamilton principle result in an eigenvalue problem

$$\mathbf{K^e X} = \mathbf{K^g X} \tag{30}$$

where $\mathbf{K^e}$ is the elastic stiffness matrix and $\mathbf{K^g}$ is the geometric stiffness matrix and is originating from the applied compressive loads. The above system is a linear eigenvalue problem which should be solved using a standard procedure to reach the critical buckling load and the buckled configuration of the plate.

**Table 2** Mechanical properties of (10,10) armchair SWCNT at reference temperature [36] (tube length = 9.26 nm, tube mean radius = 0.68 nm, tube thickness = 0.067 nm)

| $T$ (K) | $E_{11}^{CN}$ (TPa) | $E_{22}^{CN}$ (TPa) | $G_{12}^{CN}$ (TPa) | $\nu_{12}^{CN}$ |
|---|---|---|---|---|
| 300 | 5.6466 | 7.0800 | 1.9445 | 0.175 |

## 5 Numerical results and discussion

The aim beyond the present study and the developed procedure in the previous steps is to study the buckling characteristics of carbon nanotube-reinforced composite plates subjected to nonuniform compression at the boundaries. In the rest of this manuscript, the following convention is established for boundary conditions. For instance, in a CSCF plate, the first letter is associated with $x = -0.5a$, the second letter is the boundary condition at $y = -0.5b$, the third letter denotes the boundary conditions at $x = +0.5a$, and finally the last letter is associated with the boundary at $y = +0.5b$. Unless otherwise stated, poly(methyl methacrylate), referred to as PMMA, is selected for the matrix with material properties $E^m = 2.5\,\text{GPa}$ and $\nu^m = 0.34$. A (10,10) armchair SWCNT is chosen as the reinforcement. Elasticity modulus, shear modulus, and Poisson's ratio of SWCNT are dependent on temperature. However, in this study the temperature dependency of the constituents is ignored, and material properties are considered at reference temperature $T = 300\,\text{K}$. Shen and Xiang [36] reported these properties at reference temperature $T = 300\,\text{K}$. The magnitudes of $E_{11}$, $E_{22}$, $G_{12}$, and $\nu_{12}$ for CNTs at reference temperature are given in Table 2.

Han and Elliott [37] performed a molecular dynamics simulation to obtain the mechanical properties of nanocomposites reinforced with SWCNT. However, in their analysis, the effective thickness of CNTs is assumed to be at least 0.34 nm. The thickness of CNTs as reported should be at most 0.142 nm [38]. Therefore, the molecular dynamics simulation of Han and Elliott [37] is re-examined [34]. The so-called efficiency parameters, as stated earlier, are chosen to match the data obtained by the modified rule of mixtures of the present study and the molecular dynamics simulation results [34]. For three different volume fractions of CNTs, these parameters are: $\eta_1 = 0.137$ and $\eta_2 = 1.022$ for $V_{CN}^* = 0.12$, $\eta_1 = 0.142$ and $\eta_2 = 1.626$ for $V_{CN}^* = 0.17$, and $\eta_1 = 0.141$ and $\eta_2 = 1.585$ for $V_{CN}^* = 0.28$. For each case, the efficiency parameter $\eta_3$ is equal to $0.7\eta_2$. The shear modulus $G_{13}$ is taken equal to $G_{12}$, whereas $G_{23}$ is taken equal to $1.2G_{12}$ [34].

### 5.1 Comparison studies

In the present Section, comparison studies are provided to assure the validity and accuracy of the present formulation. It should be mentioned that the number of shape functions in the series expansion (25) is chosen as $N_x = N_y = 14$ after examination of convergence up to four digits.

For the first comparison study, thin isotropic plates with various types of boundary conditions are considered. In Table 3 results of our study are compared with those of Panda [4] which are obtained according to the Galerkin method whose shape function is constructed by means of the beam vibration functions and those of Wang et al. [2] which are obtained according to the generalised differential quadrature formulation. Nine different sets of boundary conditions are considered. The plate is assumed to be homogeneous and isotropic with Poisson's ratio $\nu = 0.25$. Results are confined to the case of a thin plate with $a/h = 100$. It is seen that the results of our study are in good agreement with those of Wang et al. [2] and Panda and Ramachanda [4]. However, small divergences are observed in the case of plates with moderate and high aspect ratios. This divergence is due the presence of the stress diffusion phenomenon which becomes more important in long plates.

In FG-CNTRC plates, the stiffness components $A_{i6}$, $B_{i6}$ and $D_{i6}$ are absent. Therefore, the present formulation also may be used for laminated composites with cross-ply lamination schemes. Tang and Wang [3] employed the first-order shear deformation plate theory to analyse the buckling behaviour of composite laminated rectangular plates. A comparison is performed between the results of this study and those reported by Tang and Wang [3]. A three-layer composite plate with lamination scheme [0/90/0] is considered. Properties of the layers are $E_{11} = 127.3\,\text{GPa}$, $E_{22} = 11\,\text{GPa}$, $G_{12} = G_{23} = G_{13} = 5.5\,\text{GPa}$, and $\nu_{12} = 0.34$. The plate is simply supported all around. The length-to-thickness ratio is chosen as $a/h = 100$. The buckling load factor is evaluated as a function of aspect ratio, and results are provided in Fig. 2. It is observed that the results of our study are in excellent agreement with those given by Tang and Wang [3] which guarantees the correctness of the proposed formulation and solution method.

**Table 3** Critical buckling load parameter, $\lambda_{cr} = N_{0,cr}b^2/(D\pi^2)$ for isotropic homogeneous plates with $\nu = 0.25$, $a/h = 100$ and various boundary conditions

| B.Cs. | Source | $a/b$ | | | | | | | |
|---|---|---|---|---|---|---|---|---|---|
| | | 0.4 | 0.5 | 0.6 | 0.8 | 1.0 | 1.5 | 2.0 | 3.0 |
| SSSS | Present | 9.6623 | 7.2727 | 6.0792 | 5.2102 | 5.2404 | 5.7254 | 5.5180 | 5.6100 |
| | Panda [4] | 9.654 | 7.271 | 6.078 | 5.211 | 5.242 | 5.704 | 5.478 | 5.547 |
| | Wang et al. [2] | 9.663 | 7.274 | 6.080 | 5.211 | 5.262 | 5.734 | 5.628 | 5.630 |
| SSCS | Present | 17.0086 | 12.0225 | 9.3945 | 7.0415 | 6.2726 | 6.0499 | 5.8116 | 5.7320 |
| | Panda [4] | 17.02 | 12.03 | 9.401 | 7.035 | 6.254 | 6.023 | 5.768 | 5.671 |
| | Wang et al. [2] | 17.02 | 12.03 | 9.399 | 7.045 | 6.277 | 6.058 | 5.825 | 5.756 |
| SCSS | Present | 10.0630 | 7.8873 | 6.9390 | 6.6957 | 7.5689 | 7.1201 | 7.4496 | 7.3886 |
| | Panda [4] | 10.06 | 7.877 | 6.938 | 6.692 | 7.551 | 7.104 | 7.412 | 7.373 |
| | Wang et al. [2] | 10.06 | 7.888 | 6.940 | 6.698 | 7.573 | 7.135 | 7.482 | 7.456 |
| CSCS | Present | 30.6570 | 20.9983 | 15.8183 | 10.9450 | 9.0436 | 8.1411 | 7.1031 | 6.5484 |
| | Panda [4] | 30.65 | 21.01 | 15.82 | 10.95 | 9.032 | 8.127 | 7.063 | 6.495 |
| | Wang et al. [2] | 30.69 | 21.02 | 15.83 | 10.96 | 9.054 | 8.153 | 7.123 | 6.571 |
| SCSC | Present | 10.5357 | 8.6636 | 8.0916 | 8.8850 | 9.1818 | 9.1164 | 9.0701 | 9.2234 |
| | Panda [4] | 10.52 | 8.652 | 8.087 | 8.877 | 9.172 | 9.114 | 9.053 | 9.117 |
| | Wang et al. [2] | 10.54 | 8.663 | 8.092 | 8.887 | 9.194 | 9.141 | 9.120 | 9.345 |
| SSCC | Present | 17.2817 | 12.4921 | 10.0817 | 8.2286 | 7.9644 | 7.6625 | 7.5694 | 7.4773 |
| | Panda [4] | 17.28 | 12.49 | 10.07 | 8.231 | 7.957 | 7.645 | 7.390 | 7.451 |
| | Wang et al. [2] | 17.29 | 12.50 | 10.09 | 8.233 | 7.971 | 7.679 | 7.598 | 7.544 |
| CCSC | Present | 17.5853 | 13.0519 | 10.9508 | 9.8155 | 9.8563 | 9.3636 | 9.3129 | 9.2285 |
| | Panda [4] | 17.58 | 13.04 | 10.94 | 9.814 | 9.847 | 9.340 | 8.309 | 9.205 |
| | Wang et al. [2] | 17.59 | 13.06 | 10.95 | 9.821 | 9.868 | 9.393 | 9.367 | 9.352 |
| CCCS | Present | 30.8237 | 21.3628 | 16.4192 | 12.1103 | 10.8978 | 9.7383 | 9.2096 | 8.6092 |
| | Panda [4] | 30.54 | 21.35 | 16.42 | 12.12 | 10.88 | 9.735 | 9.185 | 8.571 |
| | Wang et al. [2] | 30.58 | 21.38 | 16.44 | 12.12 | 10.91 | 9.767 | 9.246 | 8.693 |
| CCCC | Present | 31.0010 | 21.7776 | 17.1520 | 13.6988 | 13.5561 | 11.5851 | 11.1910 | 10.7853 |
| | Panda [4] | 31.01 | 21.74 | 17.15 | 13.66 | 13.55 | 11.58 | 11.17 | 10.77 |
| | Wang et al. [2] | 31.03 | 21.80 | 17.17 | 13.71 | 13.58 | 11.63 | 11.26 | 10.92 |

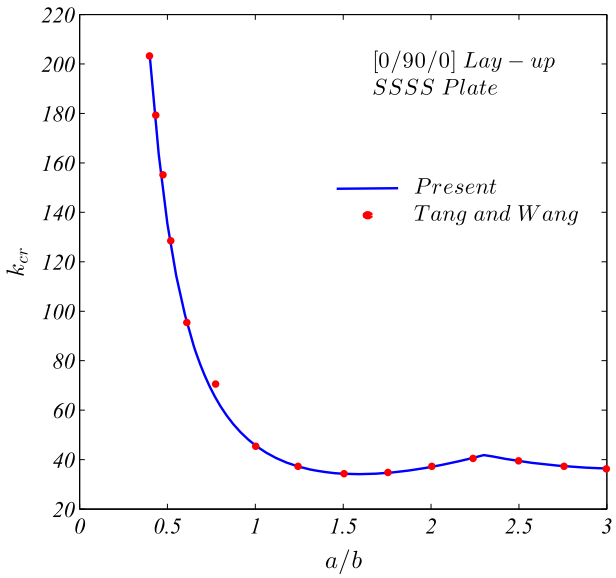


**Fig. 2** Comparison of critical buckling load parameter $k_{cr} = N_0b^2/\sqrt{D_{11}D_{22}}$ for a [0/90/0] cross-ply laminate with $a/h = 100$ and SSSS boundary conditions. Properties of the layers are $E_{11} = 127.3$ GPa, $E_{22} = 11$ GPa, $G_{12} = G_{23} = G_{13} = 5.5$ GPa, and $\nu_{12} = 0.34$. For the sake of comparison, results from Fig. 2 of Tang and Wang [3] are read from the graph

## 5.2 Parametric studies

In the whole of this Section, the critical buckling load parameter is defined as $\lambda_{cr} = N_{0,cr}b^2/(\pi^2 D_m)$ where $D_m$ is the flexural rigidity of a plate with the same thickness made of the pure polymeric matrix.

**Table 4** Critical buckling load parameter, $\lambda_{cr}$ for FG-CNTRC plates with $b/h = 50$ and $V^*_{CN} = 0.17$

| B.Cs. | Pattern | $a/b$ | | | | | | | |
|---|---|---|---|---|---|---|---|---|---|
| | | 0.4 | 0.5 | 0.6 | 0.8 | 1.0 | 1.5 | 2.0 | 3.0 |
| SSSS | UD | 263.2487 | 186.7302 | 138.9991 | 85.8715 | 59.1758 | 32.8725 | 26.0732 | 29.6035 |
| | FG-X | 353.8015 | 257.4665 | 194.6795 | 122.1227 | 84.3354 | 45.5584 | 34.2909 | 35.5179 |
| | FG-O | 153.5916 | 105.7362 | 77.4503 | 47.4787 | 33.2042 | 20.3205 | 18.3286 | 20.9085 |
| CCFF | UD | 82.1086 | 56.3175 | 41.9304 | 27.3578 | 20.1206 | 11.9494 | 9.2753 | 8.4813 |
| | FG-X | 117.1918 | 80.6285 | 59.8639 | 38.7409 | 28.4249 | 16.5968 | 12.3487 | 10.7451 |
| | FG-O | 44.9350 | 31.0450 | 23.4075 | 15.5325 | 11.5154 | 7.3203 | 6.2787 | 6.0320 |
| CFFF | UD | 81.7245 | 55.3839 | 40.3372 | 24.5427 | 16.5956 | 7.8515 | 4.5064 | 2.0273 |
| | FG-X | 116.8346 | 79.6928 | 58.1866 | 35.5386 | 24.1831 | 11.5853 | 6.6811 | 3.0154 |
| | FG-O | 44.4249 | 29.9926 | 21.8045 | 13.1404 | 8.7645 | 4.0620 | 2.3145 | 1.0357 |
| CCCF | UD | 619.8760 | 493.2057 | 396.2550 | 267.1413 | 191.2850 | 104.0320 | 70.3500 | 39.5900 |
| | FG-X | 741.9548 | 615.1019 | 510.3278 | 359.2183 | 263.4763 | 145.7887 | 98.6666 | 56.3504 |
| | FG-O | 429.1780 | 319.2504 | 244.6712 | 156.0677 | 109.1598 | 59.4595 | 40.1736 | 22.3404 |
| FCFC | UD | 3.6154 | 4.3592 | 5.2463 | 7.4560 | 10.2276 | 19.0801 | 23.1186 | 23.1133 |
| | FG-X | 4.0485 | 4.8839 | 5.8801 | 8.3643 | 11.4900 | 21.6625 | 30.7175 | 28.5792 |
| | FG-O | 3.3235 | 4.0107 | 4.8295 | 6.8607 | 9.3788 | 16.8356 | 15.7990 | 17.5136 |
| CFSF | UD | 402.0449 | 298.1997 | 227.0166 | 141.8816 | 96.3571 | 46.7927 | 28.2518 | 14.4232 |
| | FG-X | 509.0304 | 392.4508 | 307.0391 | 198.3447 | 137.0507 | 67.6319 | 40.9221 | 20.8719 |
| | FG-O | 253.1082 | 177.5351 | 130.4007 | 78.3688 | 52.2836 | 25.1201 | 15.2488 | 7.7776 |
| CCCC | UD | 619.8654 | 493.2214 | 396.3208 | 267.5472 | 192.5509 | 110.1589 | 86.6188 | 72.3625 |
| | FG-X | 741.9354 | 615.1135 | 510.3886 | 359.5975 | 264.7015 | 151.9828 | 115.2727 | 97.9234 |
| | FG-O | 429.1789 | 319.2788 | 244.7754 | 156.6488 | 110.7794 | 66.6287 | 58.1058 | 46.9493 |
| FSFS | UD | 2.2908 | 2.4506 | 2.6381 | 3.1021 | 3.6870 | 5.6601 | 8.2499 | 11.8252 |
| | FG-X | 2.5670 | 2.7472 | 2.9584 | 3.4806 | 4.1392 | 6.3699 | 9.3403 | 15.5469 |
| | FG-O | 2.0962 | 2.2431 | 2.4157 | 2.8425 | 3.3789 | 5.1624 | 7.3791 | 8.2677 |

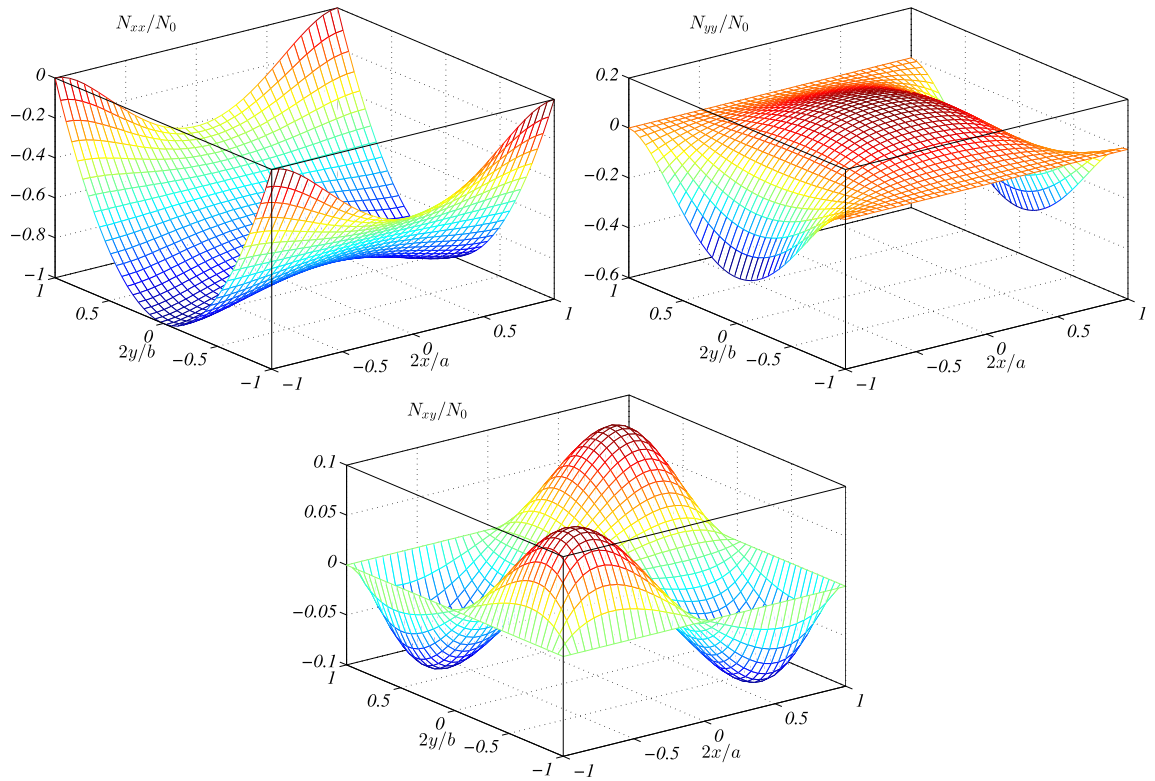


**Fig. 3** Distribution of in-plane stresses prior to buckling for a square isotropic homogeneous plate with $a/h = 100$

Table 4 presents the critical buckling load parameter of FG-CNTRC plates for three different distribution patterns, eight aspect ratios, and eight different sets of boundary conditions. The side-to-thickness ratio is set equal to $b/h = 30$, and the volume fraction of CNT is chosen as $V^*_{CN} = 0.17$. Results of this Table indicate

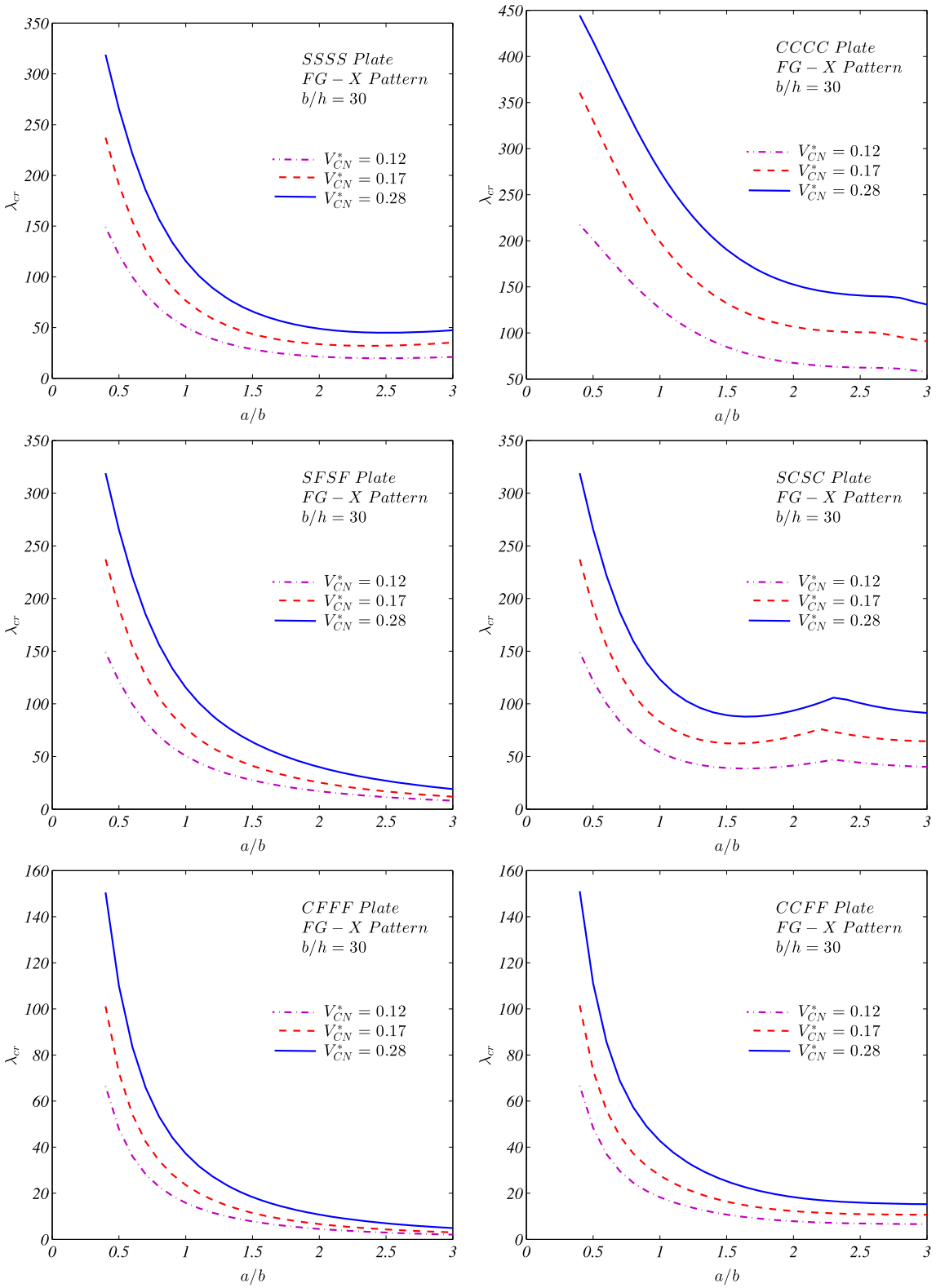


**Fig. 4** Buckling load parameter as a function of aspect ratio for FG-X CNTRC plates with $a/h = 30$, various boundary conditions, and different volume fractions of CNTs

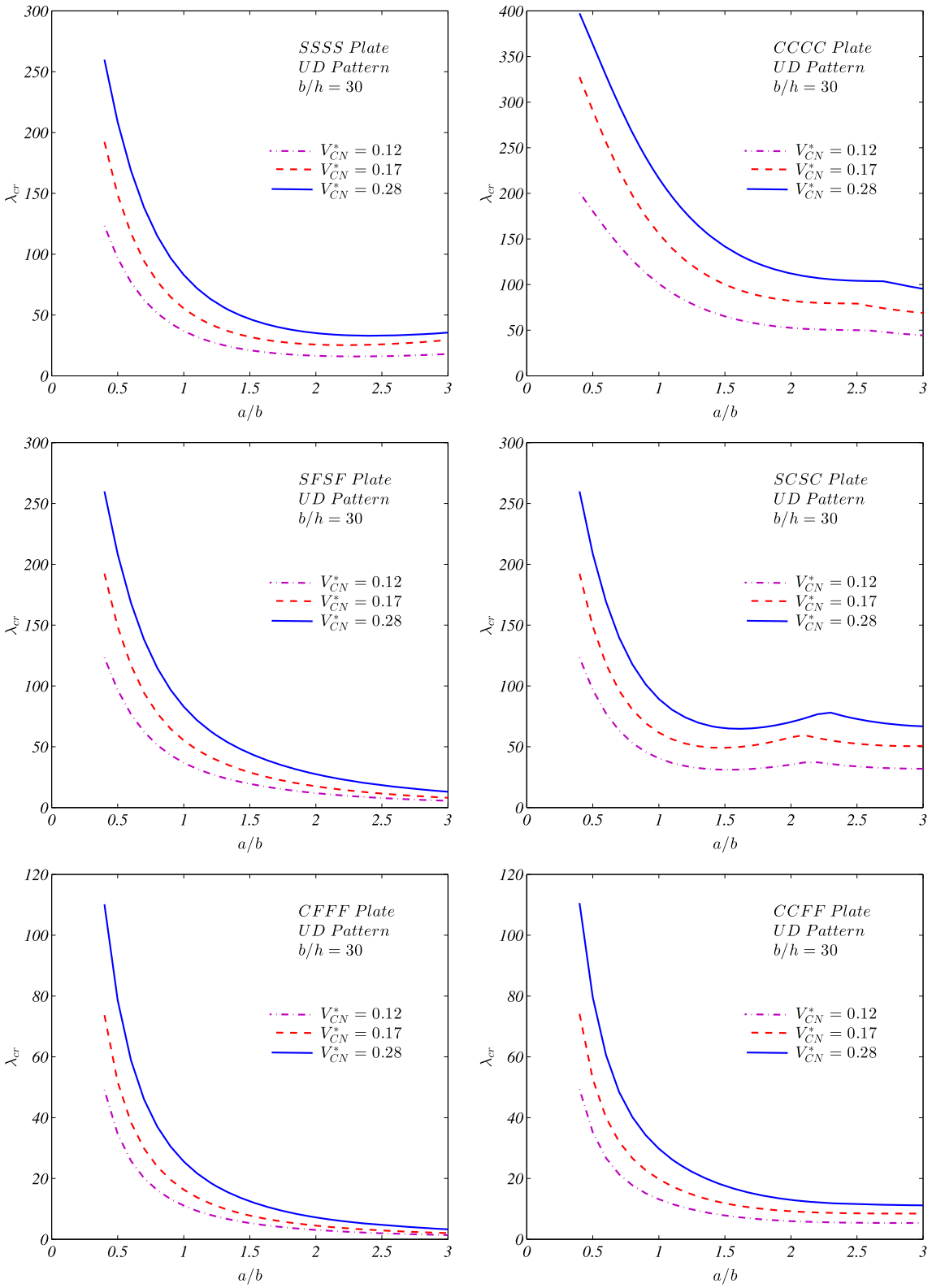


**Fig. 5** Buckling load parameter as a function of aspect ratio for UD CNTRC plates with $a/h = 30$, various boundary conditions, and different volume fractions of CNTs

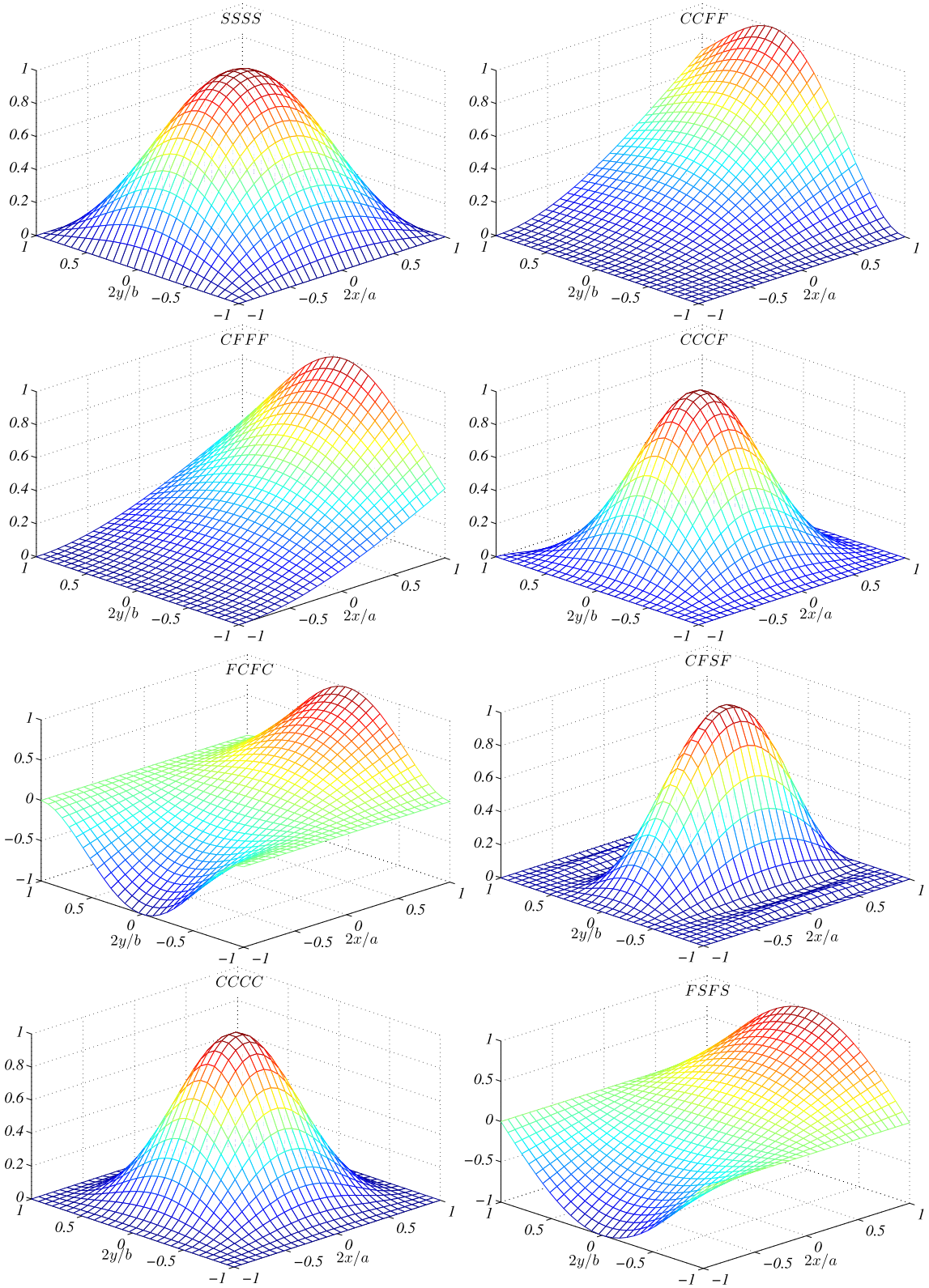


**Fig. 6** Fundamental buckling mode shape of $w_0(x, y)$ in FG-CNTRC plates with FG-X pattern, $V^*_{CN} = 0.17, a/b = 1, b/h = 50$, and various boundary conditions

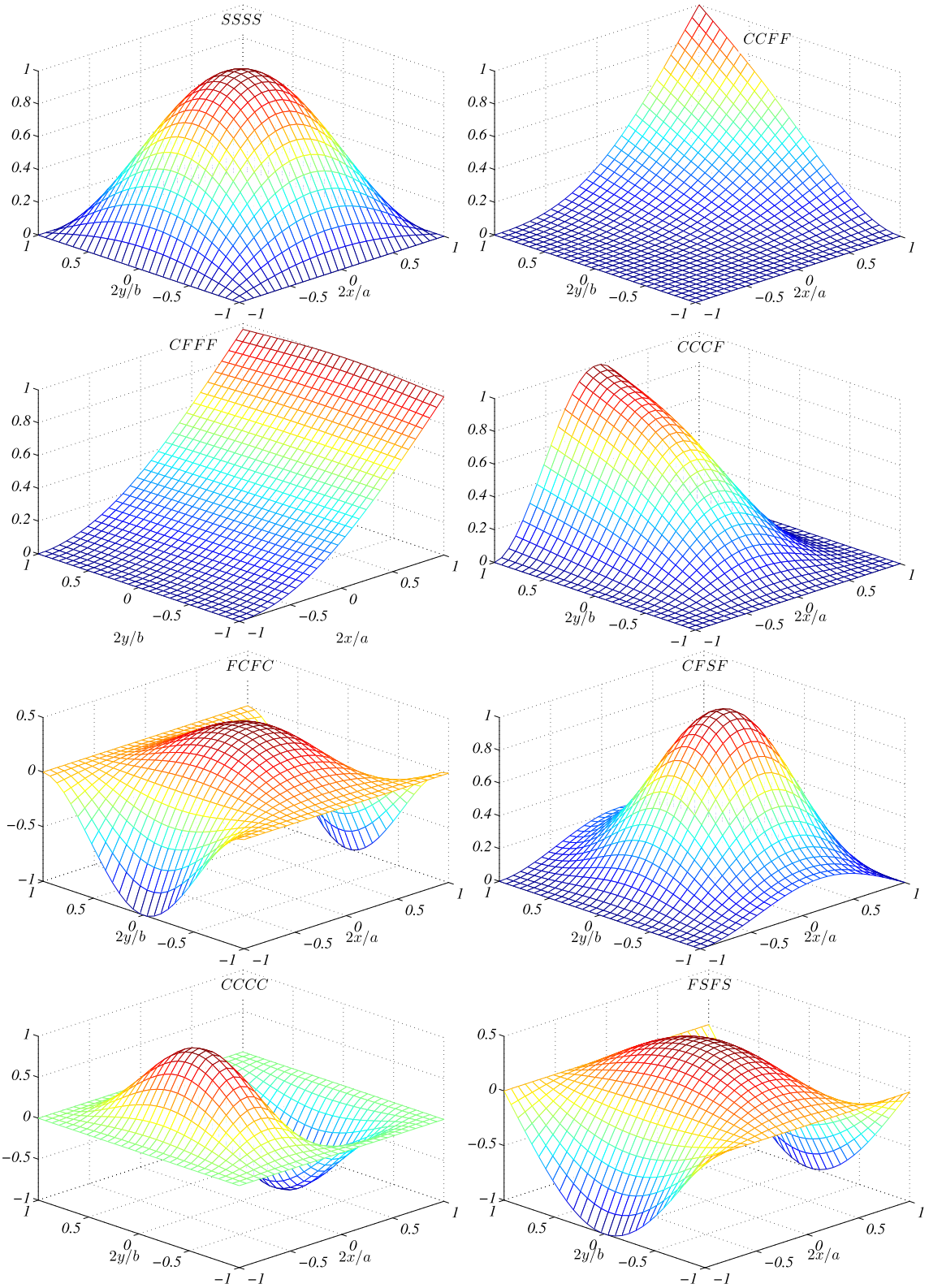


**Fig. 7** Fundamental buckling mode shape of $w_0(x, y)$ in FG-CNTRC plates with FG-X pattern, $V^*_{CN} = 0.17, a/b = 3, b/h = 50$, and various boundary conditions

that buckling loads of FG-X plates are higher than, in order, UD and FG-O plates. As expected, plates with all edges clamped have the highest buckling loads.

Figure 3 provides the in-plane stress distributions for an isotropic homogeneous plate subjected to parabolic in-plane load. It is observed that the distribution of $N_{xx}$ is different from the applied in-plane load at the edge. Furthermore, $N_{yy}$ and $N_{xy}$ are both present, and are not equal to zero. This observation is unlike the observations for plates subjected to uniform loading or the linearly varying loading. This feature is due to the stress diffusion phenomenon.

Figures 4 and 5 provide the critical buckling load parameter of FG-X and UD plates, respectively. In each Figure, six types of boundary conditions and three different volume fractions of CNTs are considered. It is verified that the buckling loads of the plate enhance as the volume fraction of CNTs increases. This effect is due to the higher elasticity modulus of CNTs in comparison with the elasticity modulus of the polymeric matrix. Comparison of the results for Figs. 4 and 5 verifies that the critical buckling load of an FG-X plate is higher than of a plate with UD pattern.

Buckling mode shapes for some selected geometrical characteristics and CNT properties are provided in Figs. 6 and 7. The presentations of these Figures are associated with the results of Table 4 with FG-X pattern. As seen from the fundamental buckling mode shape, the essential boundary conditions are satisfied at the supports. Furthermore, a comparison between the results of Figs. 6 and 7 accepts that the buckled shape of the plate is highly sensitive to the aspect ratio of the plate.

## 6 Conclusions

Most of the available works on the subject of linear stability examination of FG-CNTRC plates are based on uniform edge compression. In this research, buckling loads and mode shapes of rectangular FG-CNTRC plates subjected to parabolic edge compression are obtained using a Ritz formulation. At first, the distribution of in-plane loads within the plate domain is obtained by means of a two-dimensional formulation. Afterwards, an eigenvalue problem is formulated using the Chebyshev–Ritz method. Accuracy and correctness of the presented formulation are demonstrated by comparison with the available data for isotropic homogeneous and cross-ply laminated composite plates. Afterwards, numerical results are given for a stability analysis of FG-CNTRC plates subjected to parabolic loading. As shown, the distribution of in-plane loads within the plate is different from the applied parabolic loads at the boundary. Therefore, to reach a reliable design and to obtain the critical buckling loads, prebuckling loads should be determined accurately. It is verified that, by usage of a proper distribution of CNTs in a matrix, the buckling loads of the plate may be enhanced significantly. Furthermore, enhancement of the matrix with more CNTs results in higher buckling loads for the plate.

## References

1. Chen, X.L., Liew, K.M.: Buckling of rectangular functionally graded material plates subjected to nonlinearly distributed in-plane edge loads. Smart Mater. Struct. **13**, 1430–1437 (2004)
2. Wang, X., Wang, X., Shi, X.: Accurate buckling loads of thin rectangular plates under parabolic edge compressions by the differential quadrature method. Int. J. Mech. Sci. **49**, 447–453 (2007)
3. Tang, Y., Wang, X.: Buckling of symmetrically laminated rectangular plates under parabolic edge compressions. Int. J. Mech. Sci. **53**, 91–97 (2011)
4. Panda, S.K., Ramachandra, L.S.: Buckling of rectangular plates with various boundary conditions loaded by non-uniform inplane loads. Int. J. Mech. Sci. **52**, 819–828 (2010)
5. Ramachandra, L.S., Panda, S.K.: Dynamic instability of composite plates subjected to non-uniform in-plane loads. J. Sound Vib. **331**, 53–65 (2012)
6. Ovesy, H.R., Fazilati, J.: Parametric instability analysis of laminated composite curved shells subjected to non-uniform in-plane load. Compos. Struct. **108**, 449–455 (2014)
7. Dey, T., Kumar, R., Panda, S.K.: Postbuckling and postbuckled vibration analysis of sandwich plates under non-uniform mechanical edge loadings. Int. J. Mech. Sci. **115–116**, 226–237 (2016)
8. Panda, S.K., Ramachandra, L.S.: Buckling and postbuckling behavior of cross-ply composite plate subjected to nonuniform in-plane loads. J. Eng. Mech. **137**, 589–597 (2011)
9. Panda, S.K., Ramachandra, L.S.: Postbuckling analysis of cross-ply laminated cylindrical shell panels under parabolic mechanical edge loading. Thin Walled Struct. **48**, 660–667 (2010)
10. Liew, K.M., Lei, Z.X., Zhang, L.W.: Mechanical analysis of functionally graded carbon nanotube reinforced composites: a review. Compos. Struct. **120**, 90–97 (2015)
11. Kwon, H., Bradbury, C.R., Leparoux, M.: Fabrication of functionally graded carbon nanotube-reinforced aluminum matrix composite. Adv. Eng. Mater. **13**, 325–329 (2013)

12. Shen, H.S.: Nonlinear bending of functionally graded carbon nanotube reinforced composite plates in thermal environments. Compos. Struct. **91**, 9–19 (2009)
13. Zhang, L.W., Lei, Z.X., Liew, K.M.: Buckling analysis of FG-CNT reinforced composite thick skew plates using an element-free approach. Compos. Part B Eng. **75**, 36–46 (2015)
14. Zhang, L.W., Lei, Z.X., Liew, K.M.: Buckling analysis of functionally graded carbon nanotube-reinforced composite plates using the element-free kp-Ritz method. Compos. Struct. **98**, 160–168 (2013)
15. Malekzadeh, P., Shojaee, M.: Buckling analysis of quadrilateral laminated plates with carbon nanotubes reinforced composite layers. Thin-walled Struct. **71**, 108–118 (2013)
16. Lei, Z.X., Zhang, L.W., Liew, K.M.: Buckling of FG-CNT reinforced composite thick skew plates resting on Pasternak foundations based on an element-free approach. Appl. Math. Comput. **266**, 773–791 (2015)
17. Shen, H.S., Zhu, Z.H.: Buckling and postbuckling behavior of functionally graded nanotube-reinforced composite plates in thermal environments. Comput. Mater. Continua **18**, 155–182 (2010)
18. Shen, H.S., Zhu, Z.H.: Postbuckling of sandwich plates with nanotube-reinforced composite face sheets resting on elastic foundations. Eur. J. Mech. A Solids **35**, 10–21 (2012)
19. Shi, D.L., Feng, X.Q., Huang, Y.Y., Hwang, K.C., Gao, H.J.: The effect of nanotube waviness and agglomeration on the elastic property of carbon nanotube reinforced composites. J. Eng. Mater. Technol. **126**, 250–257 (2004)
20. Fidelus, J.D., Wiesel, E., Gojny, F.H., Schulte, K., Wagner, H.D.: Thermo-mechanical properties of randomly oriented carbon/epoxy nanocomposites. Compos. Part A Appl. Sci. Manuf. **36**, 1555–1561 (2005)
21. Jam, J.E., Kiani, Y.: Low velocity impact response of functionally graded carbon nanotube reinforced composite beams in thermal environment. Compos. Struct. **132**, 35–43 (2015)
22. Kiani, Y.: Thermal postbuckling of temperature dependent sandwich beams with carbon nanotube reinforced face sheets. J. Therm. Stress. **39**, 1098–1110 (2016)
23. Mirzaei, M., Kiani, Y.: Snap-through phenomenon in a thermally postbuckled temperature dependent sandwich beam with FG-CNTRC face sheets. Compos. Struct. **134**, 1004–1013 (2015)
24. Mirzaei, M., Kiani, Y.: Nonlinear free vibration of temperature dependent sandwich beams with carbon nanotube reinforced face sheets. Acta Mech. **227**, 1869–1884 (2016)
25. Mirzaei, M., Kiani, Y.: Thermal buckling of temperature dependent FG-CNT reinforced composite plates. Meccanica **51**, 2185–2201 (2016)
26. Mirzaei, M., Kiani, Y.: Free vibration of functionally graded carbon-nanotube-reinforced composite plates with cutout. Beilstein J. Nanotechnol. **7**, 511–523 (2016)
27. Kiani, Y.: Free vibration of carbon nanotube reinforced composite plate on point supports using Lagrangian multipliers. Meccanica. doi:10.1007/s11012-016-0466-3
28. Mirzaei, M., Kiani, Y.: Free vibration of functionally graded carbon nanotube reinforced composite cylindrical panels. Compos. Struct. **142**, 45–56 (2016)
29. Mirzaei, M., Kiani, Y.: Vibration analysis of functionally graded carbon nanotube-reinforced composite shell structures. Acta Mech. **227**, 581-559 (2016)
30. Pouresmaeeli, S., Fazelzadeh, S. A.: Frequency analysis of doubly curved functionally graded carbon nanotube-reinforced composite panels. Acta Mech. doi:10.1007/s00707-016-1647-9
31. Jam, J.E., Kiani, Y.: Buckling of pressurized functionally graded carbon nanotube reinforced conical shells. Compos. Struct. **125**, 586–595 (2015)
32. Mirzaei, M., Kiani, Y.: Thermal buckling of temperature dependent FG-CNT reinforced composite conical shells. Aerosp. Sci. Technol. **47**, 42–53 (2015)
33. Kiani, Y.: Torsional vibration of functionally graded carbon nanotube reinforced conical shells. Sci. Eng. Compos. Mater. doi:10.1515/secm-2015-0454
34. Shen, H.S.: Postbuckling of nanotube-reinforced composite cylindrical shells in thermal environments, part I: axially-loaded shells. Compos. Struct. **93**, 2096–2108 (2011)
35. Reddy, J.N.: Mechanics of Laminated Composite Plates and Shells, Theory and Application. CRC Press, Boca Raton (2003)
36. Shen, H.S., Xiang, Y.: Nonlinear analysis of nanotube reinforced composite beams resting on elastic foundations in thermal environments. Eng. Struct. **56**, 698–708 (2013)
37. Han, Y., Elliott, J.: Molecular dynamics simulations of the elastic properties of polymer/carbon nanotube composites. Comput. Mater. Sci. **39**, 315–323 (2007)
38. Wang, C.Y., Zhang, L.C.: A critical assessment of the elastic properties and effective wall thickness of single-walled carbon nanotubes. Nanotechnology **19**, 075705 (2008)